Cardiovascular Toxicology (2020) 20:401–418
https://doi.org/10.1007/s12012-020-09567-5

Exendin-4 Ameliorates Cardiac Remodeling in Experimentally Induced Myocardial Infarction in Rats by Inhibiting PARP1/NF-κB Axis in A SIRT1-Dependent Mechanism

Refaat A. Eid[1] · Samah A. Alharbi[2] · Attalla Farag El-kott[3,4] · Samy M. Eleawa[5] · Mohamed Samir Ahmed Zaki[6,7] · Fahmy El-Sayed[1] · Muhammad Alaa Eldeen[8] · Hussain Aldera[9] · Abd Al-Rahman Salem Al-Shudiefat[10]

Published online: 19 March 2020

Abstract

Sirt1 is a potent inhibitor of both poly(ADP-ribose) polymerases1 (PARP1) and NF-kB. This study investigated the cardioprotective effect of exendin-4 on cardiac function and remodeling in rats after an expreimentally-induced myocardial infarction (MI) and explored if this protection involves SIRT1/PARP1 axis. Rats were divided into five groups ($n = 10$/each): sham, sham + exendin-4 (25 nmol/kg/day i.p.), MI (induced by LAD occlusion), MI + exendin-4, and sham + exendin-4 + EX527 (5 mg/2×/week) (a SIRT1 inhibitor). All treatments were given for 6 weeks post the induction of MI. In sham-operated and MI-induced rats, exendin-4 significantly upregulated Bcl-2 levels, enhanced activity, mRNA, and levels of SIRT1, inhibited activity, mRNA, and levels of PARP1, and reduced ROS generation and PARP1 acetylation. In MI-treated rats, these effects were associated with improved cardiac architectures and LV function, reduced collagen deposition, and reduced mRNA and total levels of TNF-α and IL-6, as well as, the activation of NF-κB p65. In addition, exendin-4 inhibited the interaction of PARP1 with p300, TGF-β1, Smad3, and NF-κB p65 and signficantly reduced mRNA and protein levels of collagen I/III and protein levels of MMP2/9. In conclusion, exendin-4 is a potent cardioprotective agent that prevents post-MI inflammation and cardiac remodeling by activating SIRT1-induced inhibition of PARP1.

Keywords Exendin-4 · PARP1 · SIRT1 · NF-κb · Remodeling · Heart · Rats

Introduction

Pathological cardiac remodeling that arises post-myocardial infarction (MI) is the leading cause for the development and progression of heart failure (HF) [1]. It is a result of complicated interactions and signaling pathways between all cardiac cells including endothelial cells, myocytes, fibroblasts, and resident and infiltrating macrophages and involves a perpetuating vicious cycle of oxidative stress, sterile inflammation, sustained fibrosis and apoptosis [1], although it is a compensatory mechanism during the acute phase of MI [2]. If sustained, cardiac remodeling becomes

✉ Refaat A. Eid
refaat_eid@yahoo.com

1 Department of Pathology, College of Medicine, King Khalid University, Abha, Saudi Arabia

2 Department of Physiology, College of Medicine, Umm Al-Qura University, Mekkah, Saudi Arabia

3 Department of Biology, College of Science, King Khalid University, P.O. 641, Abha 61421, Saudi Arabia

4 Department of Zoology, Faculty of Science, Damanhour University, Damanhour, Egypt

5 Department of Applied Medical Sciences, College of Health Sciences, PAAET, Shuwaikh, Kuwait

6 Department of Anatomy, College of Medicine, King Khalid University, P.O. 641, Abha 61421, Saudi Arabia

7 Department of Histology, Faculty of Medicine, Zagazig University, Zagazig, Egypt

8 Biology Department, Physiology Section, Faculty of Science, Zagazig University, Zagazig, Egypt

9 Department of Basic Medical Sciences/College of Medicine/King Saud bin, Abdulaziz University for Health Sciences, Riyadh, Saudi Arabia

10 Department of Medical Laboratory Sciences, The Hashemite University, Zarqa, Jordan

a maladaptive mechanism that leads to several irreversible adverse effects in the structure and function of the heart which ultimately ends with HF [2–5].

Currently, an accumulating in vivo and in vitro evidence is showing an emerging role of poly(ADP-ribose) polymerases (PARPs), a group of DNA repair enzymes, in the pathogenesis of several cardiovascular disorders [6–9]. PARP1 is the most common PARPs in most eukaryotic cells including cardiomyocytes, fibroblasts, and immune cells and is usually found in the nuclei and mitochondria [10]. PARP1 contributes to about 85% of the total cellular PARPs catalytic activity [10]. It is highly expressed and activated in response to DNA damage to promote the NAD^+-dependent protein poly(ADP-ribosyl)ation (PARylation) and repair the damage [11]. Nevertheless, acylation of PARP1 at specific lysine residues is needed for full activation of the enzyme activity. In this regard, it was shown that activation of the silent information regulator 1 (SIRT1), an (NAD^+)-dependent protein deacetylase and a survival intracellular molecules, can precisely deacetylate PARP1 leading to its inactivation [12]. Moreover, SIRT1 can repress the synthesis of PARP1 by inhibting the activity of the PARP1 gene promoter [12].

However, although its main function is to repair the DNA damage, over-production/activation of PARP1 can induce cell death due to the over-consumption of NAD^+ [13]. In addition, PARP1 is one of the potent inflammatory molecules in most cells by its ability to act as a transcriptional coactivator of nuclear factor kappa light chain enhancer of activated B cells (NF-κB), a master regulator of inflammation and fibrosis [14]. Therefore, activated PARP1/NF-κB has been defined as a key player in the process of cardiac injury and remodeling that happens during and after MI. Indeed, protein levels and activity of PARP1 were significantly increased in the hearts and circulatory mononuclear cells of experimentally-induced MI and HF in rodents and were associated with increasing the inflammation, apoptosis, and fibrosis [15–17]. However, inhibition of PARP1 preserved the contractility function, reduced infarct size, inhibited hypertrophy, inflammation, and fibrosis, and reduced cell apoptosis [7–9, 16–18].

On the other hand, current studies have confirmed the importance of gut hormones in the regulation of cardiac function and protection against adverse remodeling post MI and during the development of HF [19, 20]. Glucagon-like peptide-1 (GLP-1) is the most studied gut hormone in humans and rodents [20]. It is primarily synthesized from mammalian's gut to control the appetite and satiety and was shown to have potent insulin-tropic properties by acting on peripheral GLP-1 receptors (GLP-1R) [20]. Due to its short half time, multiple synthetic GLP-1 analogs/agonists have been developed and showed much higher bioavailability and efficiency [21]. Among all, exendin-4 is the most common GLP-1 agonist, available of benches, to treat against symptoms and complications of diabetes mellitus (DM) [21].

Independent of their metabolic and glycaemic effects, a large number of experimental, preclinical and clinical studies have demonstrated therapeutic benefits of GLP-1 and exendin-4 in animals' models of diabetic cardiomyopathy (DC), ischemia, ischemia/reperfusion (I/R), MI, and HF or in patients with ischemic heart disorders and MI [20]. Indeed, administration of exendin-4 for 3 days in patients with ST-segment elevation myocardial infarction (STEMI) significantly reduced the infarct size, as assessed by cardiac MRI, and lowered serum levels of creatine kinase-MB (CK-MB) and troponin I, 38 days after reperfusion [22]. In other rodents and porcine animal models of DC, I/R injury, and MI, administration of GLP-1 or exendin-4 increased overall survival, reduced infarct size, inhibited cardiomyocytes apoptosis, improved cardiac protein expression pattern, increased cardiac output and end-diastolic volume (preload), and stimulated glucose metabolism of non-infarcted cells [21, 23–25]. In addition, exendin-4 prevented cardiac remodeling in female mice and reduced the synthesis of procollagen IaI/IIIaI, TGF-β3, and pro-inflammatory cytokines (IL-1β, IL-6) through reducing macrophage infiltration and modulating the activity of Akt/GSK-3β and Smad2/3 signaling [26]. Also, exendin-4 prevented diastolic dysfunction and cardiac inflammation in the hearts of diabetic rats by reducing the number of the infiltrating macrophages and inhibition of pro-inflammatory cytokines synthesis and releases [27].

The precise mechanisms by which exendin-4 affords its cardioprotection and prevents cardiac remodeling post MI remains challenging in light of previous studies and needs further investigation. Recently, we have shown that exendin-4 is able to preserve cardiac function, reduced infarct size, and inhibit cell apoptosis in a rat model of cardiac I/R injury by upregulation and activation of SIRT1 (data in press). Given the pro-inflammatory and fibrotic roles of PARP1 and its negative regulation by SIRT1 which is normally depressed in the heart of rats post MI [28], in this rat's study of experimentally-induced MI, we hypothesized that exendin-4 preserves cardiac function and inhibits cell apoptosis, inflammation, and fibrosis by activation of SIRT1 and inhibition of PARP1.

Materials and Methods

Animals

Adults male rats (Wistar strain) (150–155 g, 7 weeks of age) were supplied form the animal research and breading center of King Khalid University (KKU, Abha, Saudi Arabia) and were always maintained in an environmentally

controlled room (temperature of 22 ± 1 °C, the humidity of 60%, and 12-h/12-h light/dark cycles). Before the beginning of the study, all animals were adapted for 7 days. All experimental procedures including animal handling, surgical procedures, blood, and tissue collection were approved by the animal use and care ethical committee at KKU which follows the guidelines published by the US National Institutes of Health animal (NIH publication no. 85-23, revised 1996).

Animal Model of MI

Myocardial infarction was induced by permanent left anterior descending coronary artery (LAD)ligation as previously described in our laboratories [19]. Briefly, each rat was anesthetized by 1% sodium pentobarbital (50 mg/kg i.p.) and received buprenorphine-HCl analgesia (0.05 mg/kg i.m.). The rat was then ventilated and its chest was opened to expose the heart. The LAD was ligated using an 8–0 polypropylene suture. The induction of MI was confirmed by the ST elevation on the lead II of the ECG recording (AD Instruments, Sydney, Australia). The rats in the sham-operated group underwent a similar procedure but without tying the LAD. During the surgery, the temperature was monitored in all rats by an anal probe and an eye ointment was applied to prevent dryness. Post surgery, Buprenorphine analgesia and penicillin (1000 U) was administered to all rats.

Experimental Groups

All survived animals were divided into five groups ($n = 10$ rats/each) as follows (1) sham-operated group: were underwent the same surgical procedure but without tying the thread around the LAD artery; (2) sham + exendin-4 -treated group: were treated with exendin-4 (25 nmol/kg/day i.p.) (cat. no. E7144, cas no. 141758-74-9, Sigma administered, UK), (3) MI-induced group: underwent LAD ligation (4) MI + exendin-4: were rats with established MI and were administered exendin-4 (25 nmol/kg/day i.p.). (5) MI + exenatide + EX527: were MI-induced rats and were administered (25 nmol/kg/day i.p.) EX527, a selective SIRT1 inhibitor (5 mg/kg, twice per week i.p). Exendin-4 was dissolved in DMSO and diluted in PBS (pH 7.4) wherein the final concentration of DMSO was < 0.05%. As the first treatment, EX527 was administered to rats 30 min before the LAD ligation, whereas exendin-4 was initially administered at the time of the ligation. All treatments were conducted for 6 weeks. The dose of exendin-4 used in this study was based on the study of Robinson et al. [26] who showed a cardioprotective effect against MI-induced inflammation and fibrosis. However, the dose of EX527 has been used previously in rodent models of MI and HF and reported not to have any obvious cardiac adverse effects [29].

Evaluation of Cardiac Hemodynamic Parameters

At the end of weeks 6, all animals were anesthetized by 1% sodium pentobarbital (50 mg/kg i.p.) and thoracotomy was performed under ventilation. Recording of cardiac hemodynamic parameters was performed for 10 rats/group as previously described in our laboratories using a calibrated SPR-320 pressure catheter and Power lab instrument (AD Instruments, Sydney, Australia) [19]. after stabilization, data were recorded for 20 min and analyzed using Lab Chart Pro (V8) AD Instruments, Sydney, Australia) to calculate the systolic pressure increment (dP/dt_{max}) and diastolic decrement (dP/dt_{min}), the left ventricular systolic pressure (LVSP), and left ventricular end diastolic pressure (LVEDP).

Serum Preparation and Tissue Collection

Directly after hemodynamic recording, arterial blood samples were collected from the carotid artery and centrifuged at 3000×*g* for 10 min to collect sera which were stored at – 80 °C for further use. Then all animals were killed by cervical dislocation and their hearts were rapidly excised on ice. Parts of their LVs (non-infarcted myocardium) were cut fixed in 10% buffered formalin. On the other hand, other parts of the non-infarcted myocardium were placed in 2.5% glutaraldehyde (in 0.1 M sodium cacodylate buffer) or snap-frozen in liquid nitrogen and stored at – 80 °C for further use.

Determination of Cardiac Markers in the Serum

Serum levels of lactate dehydrogenase (LDH) were performed using a colorimetric kit (cat. no. ab102526, Abcam, Cambridge, UK). CK-MB and Troponin I were determined using special ELISA rat's kits (cat. no. MBS2515061, MyBioSource, CA, USA and cat. no. ab246529, Abcam, Cambridge, UK, respectively). All measurements were done for 6 rats/group in duplicate in accordance with the manufacturer's instructions.

Biochemical Analysis in the Tissue Homogenates

Frozen LVs sample of all rats was homogenized, individually, in the proper volume of ice-cold PBS (pH 7.4) supplied with a protease inhibitor cocktail (cat. no. P8340 Sigma-Aldrich, MO, USA). Levels of malondialdehyde (MDA) and Reactive oxygen/nitrogen species (ROS/RNS) in left LVs of all groups were measured using assay kits (cat. no. NWK-MDA01, NWLSS, USA, OxiSelect, cat. no. STA-347, Cell

Biolabs, Inc., San Diego, CA, and cat no. EIASODC, ThermoFisher, USA; respectively). For determination of free radicals levels, ROS and RNS species react with DCFH, which is rapidly oxidized to the highly fluorescent 2′,7′-dichlorodihydrofluorescein (DCF) that can be read using a fluorescence plate reader (FL600Bio-Tek Instruments, Inc., Winooski, VT, USA) at 480 nm excitation and 530 nm emission. LVs levels of IL-1β were determined using a rat's ELISA kit (cat. no. ab100767, Abcam, UK). Tissue levels of TNF-α and IL-6 levels were measured using ELISA kits (cat. no. CSB-E11987r and CSB-E04640r, CUSABIO technology LLC, TX, USA). All measurements were done for 6 rats/group in duplicate in accordance with the manufacturer's instructions.

Isolation of the Total, Nuclear and Cytoplasmic Proteins

To prepare total cell homogenates, frozen LVs samples (30 mg) were homogenized in 500 µl RIPA buffer containing 50 mM Tris (pH 8.0), 150 mM sodium chloride 0.5% sodium deoxycholate; 0.1% SDS, 1.0% NP-40, and protease inhibitor cocktail (cat. no. P8340, Sigma-Aldrich, St. Louis, MO, USA). The nuclear and cytosolic protein fractions were prepared using CelLytic NuCLEAR Extraction Kit (cat. no. NXTRACT, Sigma-Aldrich, St. Louis, MO, USA). In brief, frozen LV tissue (25 mg) was homogenized in 500 µl lysis buffer (50 mM Tris–HCl (pH 7.5), 10 mM $MgCl_2$, 15 mM $CaCl_2$, and 1.5 M Sucrose) plus 5 µl of 0.1 M DTT and 5 µl of protease inhibitor cocktail (cat. no. P8340, Sigma-Aldrich, St. Louis, MO, USA), centrifuged at 4 °C at a speed of 11,000×*g* for 20 min. The supernatants (systolic proteins) were transferred to a new tube and stored at – 20 °C until use. The remaining pellet was suspended in 150 µl of extraction buffer containing 147 µl of the extraction solution (20 mM HEPES (pH 7.9), 0.2 mM EDTA, 1.5 mM $MgCl_2$, 25% (v/v) Glycerol and 0.42 M NaCl) plus1.5 M DTT and 1.5 µl protease inhibitor cocktail and incubated on a shaker 4 °C for 30 min. The tubes were centrifuged at 4 °C at 20,000×*g* for 5 min and the supernatants (nuclear proteins) were collected and stored at − 20 °C until the time of the analysis. The protein concentrations in the supernatants of all samples were measured using a Pierce BCA Protein Assay Kit (cat. no. 23225, ThermoFisher Scientific). Protein levels of Lamine B and β-tubulin were detected by western blotting to ensure the purities of the nuclear and cytoplasmic fractions, respectively.

Biochemical Measurements in the Nuclear Fraction

SIRT1 deacetylase activity was measured using a fluorometric Cyclex SIRT1/Sir2 Deacetylase Fluorometric Assay Kit (cat. no. CY-1151V, Nagano, Japan) using 20 µg of the nuclear extract. The test is based on the ability of SIRT1 to deacetylase and activate peptidase which then cleave fluorophore peptide substrate to emit the fluorescent signal that can be read test at 2 min time intervals after 30–60 min using a microplate fluorescence reader (FL600Bio-Tek Instruments, Inc., Winooski, VT, USA) at an excitation at 340 nm and emission at 460 nm. Nuclear PAR-1 activity was measured by the universal colorimetric using 25 µg of the nuclear extract. PARP assay kit (cat. no. 4677-096-K, Gaithersburg, MD, USA) based on the incorporation of biotinylated ADP-ribose onto histone proteins and interaction with HRP-specific antibody. The absorbance was read using read at 450 nm at 405 nm with a Spectramax microplate reader. The activation of p65 in the nuclear fractions was measured using the ELISA-based kit, Trans AM assay kit (cat. no. 40596, Active Motif, Tokyo, Japan) using 20 µl (20 µg) of the nuclear extract. The test is based on the detected amount of p65 bounded to oligonucleotides by specific antibodies and HRP secondary antibodies. Absorbance was read at 450 and the activation of p65 was calculated using a standard curve generated using a recombinant NF-kB p65 (cat. no. 31102, Active Motif, Tokyo, Japan). All measurements were done for 6 rats/group and all procedures were performed in accordance with the manufacturer's instructions.

Table 1 Primers pairs used in the real-time PCR

Gene	Accession	F: sequence (5′ → 3′)	R: (5′ → 3′)	bp
SIRT1	XM_003751934.1	GTTCTGACTGGAGCTGGGGT	ATGGCTTGAGGATCTGGGAG	119
COLI	NM_017051	TTCACCTACAGCACGCTTGT	TGGGATGGAGGGAGTTTAC	196
COLIII	NM_017059	GGTCACTTTCACTGGTTGACGA	TTGAATATCAAACACGCAAGGC	201
PARP1	NM_013063	CGCTCAAGGCTCAGAACGAG	CAGGATTGCGGACTCTCCA	130
TNF-α	NM_012675.3	AGAACAGCAACTCCAGAACACCCT	TGCCAGTTCCACATCTCGGATCAT	160
IL-6	NM012589.1	GTGGAAGACAAACCATGTTGCCGT	TATTGCAGGTGAGCTGGACGTTCT	116
TGF-β1	NM_021578.2	GGCGGTGCTCGCTTTGTA	GGGTGACTT CTTTGGCGTAG	104
β-Actin	NM_031144.2	TACCCAGGCATTGCTGACAG	AGCCACCAATCCACACAGAG	115

Quantitative RT-PCR

Quantitative real-time PCR was used to measure the mRNA levels of SIRT1, PRAP1, Collagen I α1 (Col Iα1), ColIIIα, TNF-α, TGF-1β, IL-6, and ß-actin. Primer sequences were previously shown in similar studies [30–34] and are presented in Table 1. Total RNA from frozen LVs samples (40 mg) were extracted using An RNeasy Mini Kit (cat. no. 74104, Qiagen, VIC, Australia). The purity of the isolated RNA was determined by taking the absorbance at 260/280 using a Nanodrop spectrophotometer. The first-strand cDNA for all samples was synthesized using iScript cDNA synthesis kit (Bio-Rad). qPCR runs were performed in CFX96 real-time PCR system (Bio-Rad, CA, USA) using Ssofast Evergreen Supermix (cat. no. 172-5200, Bio-Rad, Montreal, Canada). Briefly, 2 µl of diluted cDNA, 10 µl of SYBR green master mix, 0.15 µl of 10 µM forward and reverse primers, and 7.7 µl of nuclease-free water were added for each reaction. The qPCR run consisted of (1) enzyme inactivation for 30 s at 95 °C, (2) denaturation at 95 °C for 5 s, (3) annealing/extension at 60 °C for 30 s, and (4) melting at 95 °C for 1 s. Steps 2 and 3 were carried out for 35 cycles and steps 1 and 4 were performed as 1 cycle. The relative expression of each target gene was calculated using the comparative cycle threshold (C_t) method ($2^{-\Delta\Delta C_t}$). False detection with the qPCR was controlled by adding and testing a no-template-control on every run for each primer used and checking the melting curves. All measurements were done for 6 rats/group.

Immunoprecipitation of Acyl PPAR-1

Nuclear proteins (100 µg) of each sample was diluted in 500 µl lysis buffer (20 mM HEPES, 0.1% NP-40, 75 mM KCl, 2.5 mM $MgCl_2$, and 1 mM DTT plus 5 µl protease inhibitor cocktail (cat. no. P8340, Sigma-Aldrich, St. Louis, MO, USA). Then, 20 µl of 50% protein-A/G plus-agarose and 2 µg of rabbit IgG (Santa Cruz Biotechnology) prepared in the lysis buffer were added. The samples were incubated on a shaker for 2 h at 4 °C, centrifuged at 1000×*g*, and the supernatants were collected. For the isolated supernatants, 4 µg of PPAR-1 (cat. no. 9452, 1:1000, Cell Signalling Biotechnology, USA) or normal rabbit IgG were added and incubated overnight at 4 °C with shaking. Then, 30 µl of 50% of protein-A/G plus-agarose was added to each sample and incubated for 1 h at 4 °C. After that, the Protein-A/G plus-agarose beads were washed 5 times with 500 µl protein lysis buffer and incubated4°C for 5 min. Then, 30 µL 2 × Laemmli buffer was added to each tube to elute the precipitated complexes which were then boiled for 5 min before and processed for western blotting to detect protein levels of acyl-PARP1, SIRT1, P-300, and acyl p65.

Western Blotting Analysis

Equal proteins (40 µg) from the total and nuclear fractions were electrophoresed on 8–12% SDS-polyacrylamide gel and then electroblotted onto nitrocellulose membranes (Sigma). Membranes were then blocked with 5% non-fat milk, washed with TBST, and incubated at room temperature, on rotatory machine for 2 h, with the primary antibodies (depending on the target experiment) against SIRT1 (cat. no. 8469, 120 kDa, 1:250), NF-κB p65 (cat. no. 3034, 65 kDa, 1:1000), Collagen 1A1 (cat. no. 84336, 220 kDa 1:250), Bax (cat. no. 2772, 20 kDa, 1:1000), cleaved caspase-3 (cat. no. 9661, 17/19 kDa, 1:1000), PARP1 (cat. no. 9532, 116 kDa, 1:1000), p300 (cat. no. 86377, 300 kDa, 1:500), lamin B1 (cat. no. 12586, 68 kDa, 1:1000) (Cell Signalling Biotechnology), MMP9 (cat. no. sc-393859, 92 kDa, 1:1000), MPP-2 (cat. no. sc-13595, 72 kDa, 1:1000); collagen IIIA1 (cat. no. sc-271249, 110 kDa, 1:250), Bcl-2 (cat. no. sc-7382, 26 kDa, 1:1000), TGF-β1 (cat. no. sc-130348, 1:1000), IL-6 (sc-57315, 21 kDa, 1:1000), TNF-α (cat. no sc-52746, 17 kDa, 1:1000), and β-actin (cat. no. sc-47778, 45 kDa, 1:2000) (Santa Cruz Biotechnology, USA), and Acetyl PARP1 (K521, cat. no. ITK0091, 1:250) (G-Bioscience, USA). Membranes were then washed 3 times with TBST and then incubated with appropriate corresponding horseradish peroxidase (HRP)-conjugated secondary antibody. All membranes were stripped up to 5 times and band intensities were detected using a Pierce ECL kit (ThermoFisher, USA, Piscataway, NJ), scanned using C-Di Git blot scanner (LI-COR, NE, USA) and analyzed using the scanner associated software.

Histopathology and Transmission Electron Microscopy (TEM) Evaluation

Left ventricle fresh tissues were fixed in 10% buffered formalin for 48 h. The samples were routinely processed and embedded in paraffin. Sections were cut in small sections (5 µm) and then stained with hematoxylin and eosin. Other paraffin-embedded sections were stained using Trichrome Stain Kit (cat. no. ab150686, Abcam, Cambridge, UK) where muscles are stained red and collagen is stained blue. All sections were examined by a pathologist, who is unaware of the treatment groups, under a light microscope (Celestron 44341 LCD Digital Microscope II). The TEM study was performed as previously described in our studies [19].

Statistical Analysis

Statistical analysis for all measured parameters was done using Graph Pad Prism statistical software package (version 6). Differences among the experimental groups were assessed by one-way ANOVA, followed by Tukey's test. Data were presented as mean ± SD. Values will be considered significantly different when $P < 0.05$.

Results

Exendin-4 Improved Cardiac Contractility and Relaxation and Lowered Serum Cardiac Parameters in MI-Induced Rats

Left ventricles hemodynamic parameters and serum levels of cardiac markers are shown in Table 2. There were no significant differences in all measured parameters between sham-operated and sham-operated exendin-4-treated rats. MI-induced rats showed a significant increase in LV values of LVEDP and serum levels of LDH, CKMB and Troponin T with a parallel decrease in the values of LVSP, dp/dt_{max}, and dp/dt_{min} as compared to sham-operated rats (Table 2). On the other hand, MI + exendin-4-treated rats showed a significant increase in LVSP, dp/dt_{max}, and dp/dt_{min} and a significant decrease in LVEDP and serum levels of all measured cardiac markers as compared to MI-induced rats (Table 2). However, except for LVSP, the levels of these parameters remained slightly different as compared to control rats. Interestingly, MI + exendin-4 treated + EX527-treated rats similar values of all these parameters to that seen in MI-induced rats, suggesting that the protective effect of exendin-4 on heart function is SIRT1 dependent and involves suppression of cell death (Table 2).

Exendin-4 Reduced LV Inflammation by Suppressing NF-κB Activation and Inflammatory Cytokines Levels in MI-Induced Rats Through a SIRT1-Dependent Mechanism

Normal cardiac architectures were seen in sham-operated and sham + exendin-4 treated rats (Fig. 1a, I, II). There was also no significant change in the homogenate levels or, mRNA and protein levels of TNF-α and IL-6 and showed no signifcant change in the nuclear activity and levels of NF-κB p65 when sham + exendin-4 rats were compared with sham-operated rats (Figs. 1b–d, 2a, b). However, MI-induced rats showed increased aggregation of inflammatory cells with increased presence of necrotic and apoptotic cells (Fig. 1a, III, IVC). They also showed a significant increase in the homogenate levels and mRNA and protein levels of TNF-α and IL-6 (Fig. 1b–d) with a concomitant increase in the nuclear activity and protein levels of NF-κB p65 (Fig. 2a, b) in their LVs as compared to sham-operated rats (Fig. 1b–d). On the contrary, MI + exendin-4-treated rats showed significant improvement in cardiac architectures with reduced number of inflammatory, necrotic and apoptotic cells (Fig. 1a, V, VI) and had lower homogenate levels and mRNA and protein levels of TNF-α and IL-6, and had a signifcant reduction in the nuclear activity and levels of NF-κB p65 when compared to MI-induced rats (Figs. 1b–d, 2a, b). Similar histological changes with an increased number of inflammatory, necrotic and apoptotic cells and a similar increase in all these biochemical endpoints were seen in MI + exendin-4 + Ex527 when compared to MI-treated rats, thus suggesting that the anti-inflammatory effect of exendin-4 is SIRT1 dependent (Figs. 1a–d, 2a, b).

Table 2 Cardiac hemodynamic parameters and serum markers in all groups of rats

	Sham	Sham + exendin-4	MI	MI + exendin-4	MI + exendin-4 + EX527
LVSP (mmHg)	102 ± 11	108 ± 10*	64 ± 7***$^{\#\#\#}$	97 ± 5$^{\$\$\$}$	59 ± 8***$^{\#\#\#\&\&\&}$
LVEDP (mmHg)	4.1 ± 0.78	3.9 ± 0.54	12 ± 1.5***$^{\#\#\#}$	7.4 ± 0.83*$^{\#\$\$\$}$	14 ± 2.8***$^{\#\#\#\&\&\&}$
dp/dt_{max} (mmHg)	5345 ± 351	6015 ± 432*	2634 ± 227***$^{\#\#\#}$	4599 ± 319*$^{\#\$\$\$}$	2245 ± 313***$^{\#\#\#\&\&\&}$
dp/dtmin (mmHg)	4844 ± 372	5624 ± 364*	2467 ± 218***$^{\#\#\#}$	3988 ± 169*$^{\#\$\$\$}$	2689 ± 244***$^{\#\#\#\&\&\&}$
LDH (U/l)	43.8 ± 6	47.2 ± 8	453 ± 16***$^{\#\#\#}$	91.2 ± 7**$^{\#\#\$\$\$}$	423 ± 22***$^{\#\#\#\&\&\&}$
CK-MB (pg/ml)	213 ± 15	209 ± 11	643 ± 18***$^{\#\#\#}$	338 ± 13**$^{\#\#\$\$\$}$	581 ± 19***$^{\#\#\#\&\&\&}$
Troponin T (pg/ml)	185 ± 5	179 ± 12.1	478 ± 14 ***$^{\#\#\#}$	265 ± 15**$^{\#\#\$\$\$}$	463 ± 17***$^{\#\#\#\&\&\&}$

Data are presented as mean ± SD of $n = 10$ rats/group. *, *****: vs. sham at $P < 0.05$, $P < 0.01$ and 0.001, respectively. $^{\#\#,\#\#\#}$: vs. sham + exendin-4-treated rats at $P < 0.01$ and 0.001, respectively. $^{\$\$\$}$: vs. MI-induced rats at $P < 0.001$. $^{\&\&\&}$: vs. MI + exendin-4-treated rats at $P < 0.001$. EX527: a selective SIRT1 inhibitor

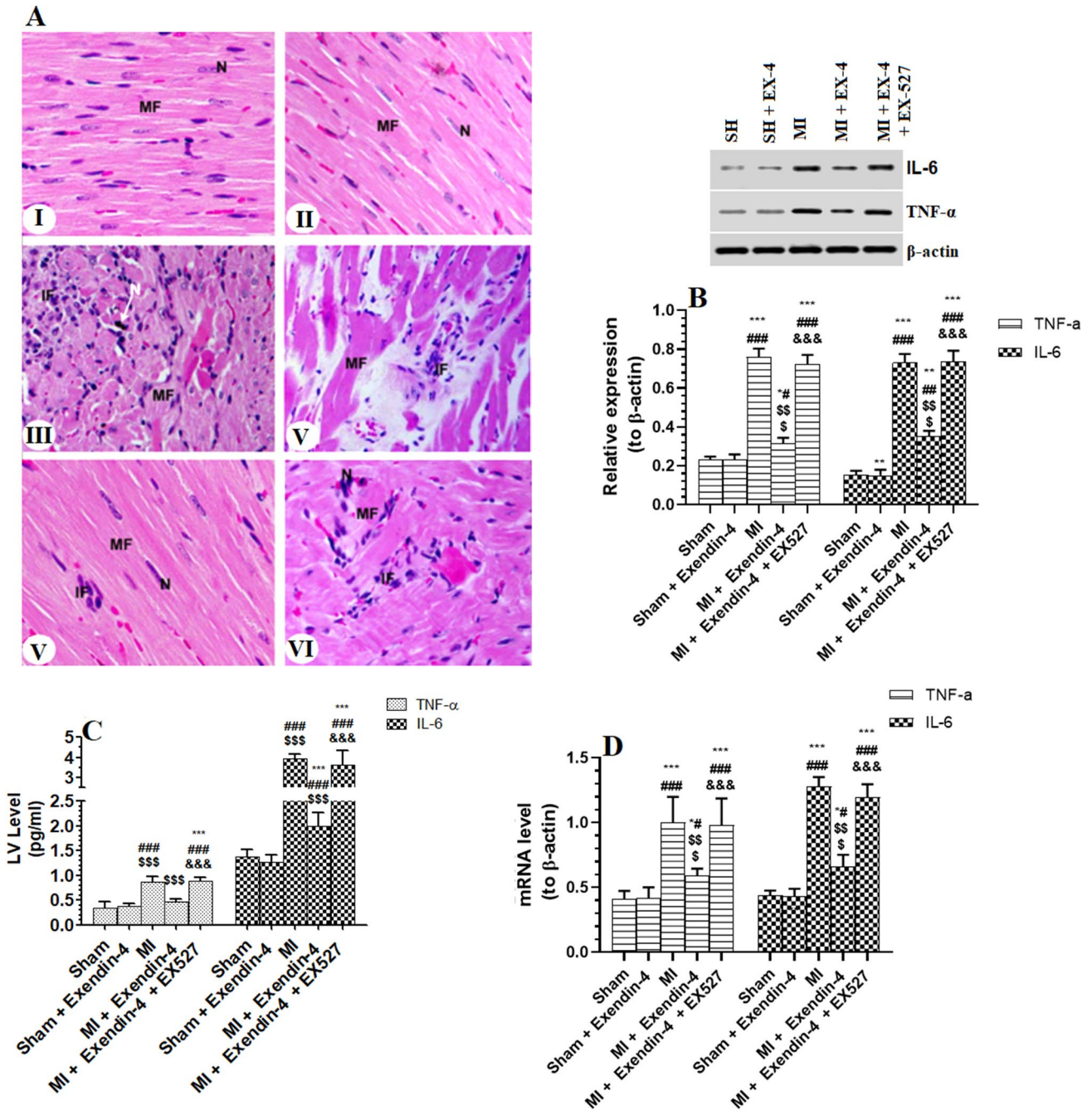

Fig. 1 Histopathology images of left ventricles (LVs) of all groups of rats (**a**) and homogenates (**b**), mRNA (**c**), and protein levels of TNF-α and IL-6 (**d**) in LVs of all groups of rats. **a** I, II were taken from the sham-operated and sham + exendin-4-treated rats, respectively, showing normal cardiac muscle cells (MF) with intact nuclei (N) and branched fibers (black arrows). III and IV were taken from MI-induced rats and show the presence of pyknotic nuclei (N), aggregation of inflammatory cells (IF), and fragmentation of myocardial tissue (MF). V was taken from MI + exendin-4-treated rats and shows normal nuclei (N) and normal myofibrils (MF) with few numbers of inflammatory cells (IF). **f** was taken from an MI + exendin-4 + EX527-treated rat and shows similar architecture to those seen in MI-induced rats. **b**–**e** Data are presented as mean ± SD of n = 6 rats/group. *, **, ***: vs. sham at $P < 0.05$, $P < 0.01$, and 0.001, respectively. $^{\#, \#\#\#}$: vs. sham + exendin-4-treated rats at $P < 0.05$, and 0.001, respectively. ^{SSS}: vs. MI-induced rats at $P < 0.001$. $^{\&\&\&}$: vs. MI + exendin-4-treated rats at $P < 0.001$. EX527: a selective SIRT1 inhibitor

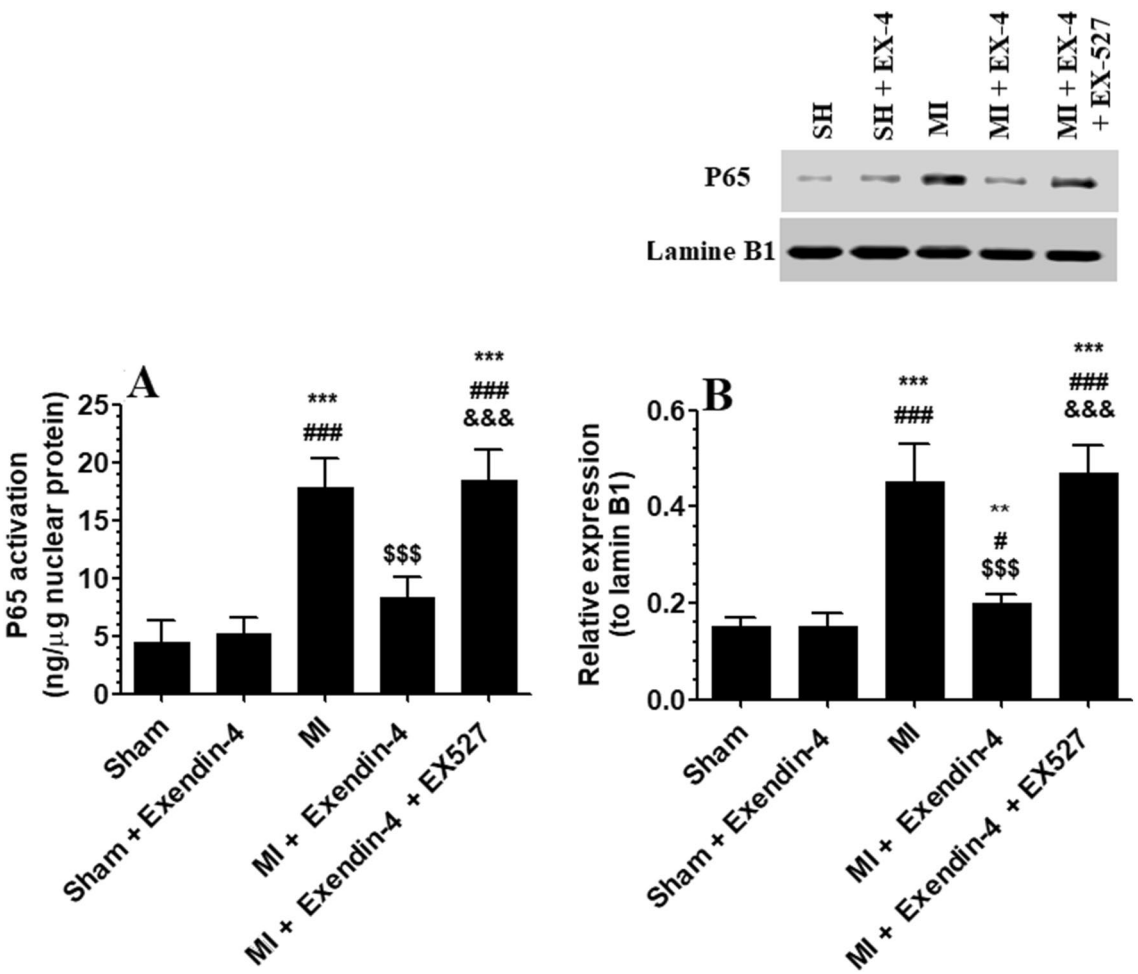

Fig. 2 The activity and protein levels of NF-κB p65 in LVs of all groups of rats. Data are presented as mean ± SD of $n = 6$ rats/group. *, **, ***: vs. sham at $P < 0.05$, $P < 0.01$,and 0.001, respectively. $^{\#,}$ $^{\#\#\#}$: vs. sham + exendin-4-treated rats at $P < 0.05$ and 0.001, respectively. ^{SSS}: vs. MI-induced rats at $P < 0.001$. $^{\&\&\&}$: vs. MI + exendin-4-treated rats at $P < 0.001$. EX527: a selective SIRT1 inhibitor

Exendin-4 Inhibited LV Collagen Synthesis in the LVs of MI-Induced Rats Through a SIRT1-Dependent Mechanism

Administration of exendin-4 to sham-operated rats didn't affect LVs levels of collagen deposition (Fig. 3aI, II), and mRNA or protein levels of collagen I/III (Fig. 3b, c). The increased amount of collagen deposition (Fig. 3aIII, aIV) with parallel increase in mRNA and protein levels of collagen I/III were seen in LVs of MI-induced rats as compared to sham-operated rats (Fig. 3b, c). However, there was a significant reduction in collagen accumulation as well as in mRNA and protein levels of collagen I/III in LVs of exendin-4 + MI + exendin-4 as compared to MI-induced rats (Fig. 3aV, b, c). All these effects of exendin-4 in MI rats were completely reversed by co-administration of EX527 and their levels in this group of rats were not significantly different from those measured in MI-induced rats (Fig. 3aVI, b, c). These data suggest that the anti-fibrotic effect of exendin-4 is SIRT1 dependent.

Exendin-4 Inhibited LV Collagen Deposition, Preserved Mitochondria, and Myofibrils Structures, and Inhibited Metalloproteinases (MMPs) and TGF-β1/Smad3 Activation in the LVs of MI-Induced Rats Through a SIRT1-Dependent Mechanism

Ultrastructural images showed intact myofibrils and mitochondria with few collagen fibers in the LVs of sham + exendin-4 treated rats as compared to sham-operated rats (Fig. 4aI, II). Also, there was no significant difference in protein levels of MPP-2, MMP9, TGF-β1, and Smad3 between these two groups of rats (Fig. 4b, c). However, electron microscopy images showed increased fragmentation of myofibrils and muscle bands, disintegrated mitochondria

and increasing amounts of collagen fibers in the LVs of MI-induced rats as compared to sham-operated rats (Fig. 4aIII, IV). The LVs of MI-induced rats also showed increased protein levels of MPP-2, MMP9, TGF-β1, and Smad3 as compared to sham-operated rats (Fig. 4b, c). on the other hand, similar changes in the ultrastructure of LVs and an increase in protein levels of MPP-2, MMP9, TGF-β1, and Smad3 to those seen in MI-induced rats have been also seen in MI + exendin-4 + EX527-treated rats (Fig. 4aV, VI, b, c).

Exendin-4 Stimulated SIRT1 Level and Activity and Simultaneously Inhibited PARP1 Level and Activity in the LVs of MI-Induced Rats

The activity of SIRT1 and mRNA and protein levels of SIRT1 were significantly decreased, whereas the activity and mRNA and protein levels of PARP1 were significantly increased in LVs of MI-induced rats as compared to sham-operated rats (Fig. 5a–f). On the other hand, the administration of exendin-4 to both sham-operated and MI-induced rats significantly increased activity and mRNA and protein levels of SIRT1 and concomitantly inhibited the activity, mRNA and protein levels of PARP1 as compared to sham-operated and MI-induced rats, respectively (Fig. 5a–f). However, activity and mRNA and protein levels of PARP1 were significantly increased in MI + exendin-4 + EX527 as compared to MI + exendin-4-treated rats and their levels were not significantly different as compared to MI-induced rats (Fig. 5d–f).

Exendin-4 Inhibited Cell Death and the Association of PARP1 with p300 and Stimulated the Association of PARP1 with SIRT1

As shown in Fig. 6a, protein levels of Bcl-2 were significantly increased and protein levels of Bax were significantly decreased in LVs of sham + exendin-4-treated rats as compared to sham-operated rats. In addition, when PARP1 was immunoprecipitated and blotted with antibodies against SIRT1, p300 and acyl-PAPR-1, LVs of the sham + exendin-4-treated rats showed a significant increase in the reactivity of SIRT1 and lower protein levels of Acyl-PARP1 (Fig. 6b). However, protein levels of Bax and cleaved caspase-3, acyl-PARP1 and interaction of PARP1 with p300 were significantly increased but protein levels of Bcl-2 and interaction of SIRT1 with Acyl-PARP1 were significantly decreased in LVs of MI-treated rats as compared with sham-operated rats (Fig. 6a, b). All these events were reversed in the LVs of MI + exendin-4-treated rats as compared to MI-induced rats (Fig. 6a, b). On the other hand, similar changes in all these parameters were seen when sham + exendin-4 + EX527 were compared with MI-induced rats (Fig. 6a, b). These data suggest that exendin-4 and through increasing SIRT1 levels inhibits cell apoptosis and acetylation of PARP1 and its interaction with p300 and stimulates the interaction of SIRT1 with PARP1.

Discussion

The findings of this study are unique to describe a mechanistic protective effect of exendin-4 against adverse cardiac remodeling post experimentally-induced MI in rats. In this study, we are showing that chronic exendin-4 treatment for 6 weeks post MI preserved the cardiac contractility, morphology, and ultra-structures of affected rats by inhibiting LV myocytes and markers of apoptosis, fibrosis, and inflammation. These effects were associated with SIRT1-induced down-regulation, deacetylation and inactivation of PARP1, a weaker PARP1/p300 interaction, and deacylation and inhibition of NF-κB p65. Of note, EX527, a selective inhibitor of SIRT1 completely abolished all the protective effects of exendin-4 and was associated with sustained inflammation and fibrosis with a concomitant increase in the activity and acetylation of NF-κB p65 and PARP1and enhanced PARP1/p300 interaction (Fig. 7).

Cardiac remodeling post MI is a major cause for the progression to HF and is usually associated with electro-mechanical disturbances, expansion of the infarct tissue, changes in the geometry of the heart, and reduced LV function [1, 2]. In both patients and animals, cardiac remodeling is characterized by an increase in LV diameter and end-diastolic pressure (LVEDP) and parallel a decrease in LV systolic pressure (LVSP) and ejection fractions [19, 35, 36]. Histological and ultrastructural changes post MI are also well described and showed severe myofibrils degeneration, mitochondria damage, lack of normal muscle striations, and vacuolization, and accumulation of collagen fibers [19].

In this study, the first evidence for the cardioprotective effect of chronic administration of exendin-4 for 6 weeks against MI-induced cardiac damage was shown by the attenuation of both systolic and diastolic functions of the LVs, improvements in LVs morphology, and preservation of myofibrils and mitochondria structures. These findings are similar to those reported by Robinson et al. [26] who showed that an 8-week treatment with exendin-4, at a similar dose in female mice model of MI, increased the overall survival rate, reduced infarct area, and preserved normal contractile function. In addition, they are supported by many other clinical and experimental studies that showed the ability of GLP-1 and exendin-4 to mitigate cardiac dysfunction [21–24].

Overproduction of ROS and increased cardiomyocytes death by apoptosis, autophagy, and necrosis in the non-infarcted myocardium are believed to be the key mechanisms that initiate all other cellular processes of cardiac remodeling including hypertrophy, inflammation, fibrosis,

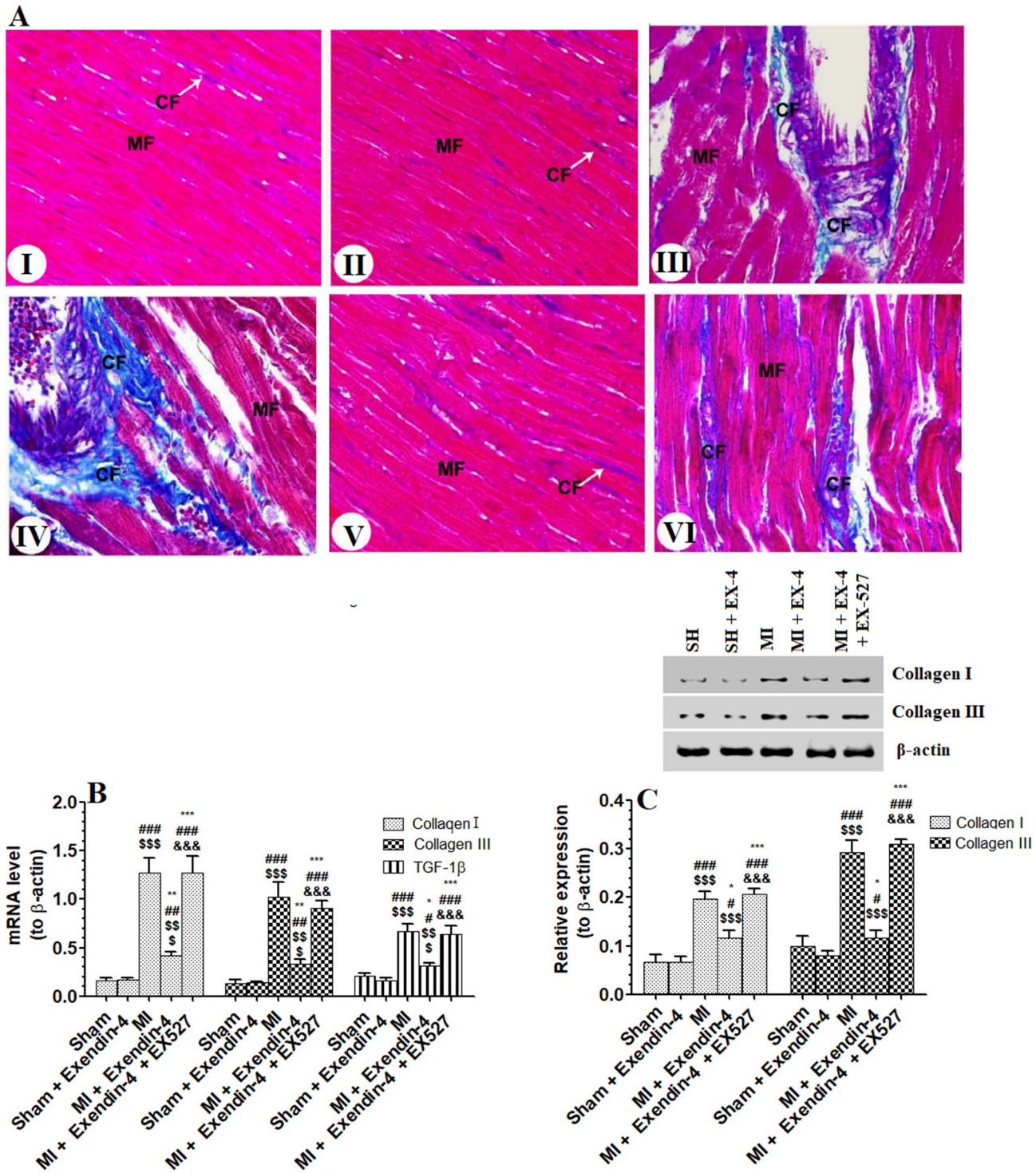

and contractile dysfunction [37]. Here, it seems very logical that the improvement in cardiac hemodynamic parameters in MI + exendin-4 treated rats of this study is a secondary increase in cell survival in the non-infract myocardium. With the obvious improvement in the mitochondria and myofibrils structures in MI-treated rats, exendin-4 also suppressed ROS generation and down-regulated markers of intrinsic apoptosis (Bax and cleaved caspase-3). Concomitantly in increased protein levels of Bcl-2 and enhanced mRNA and protein levels of the anti-oxidant genes (MnSOD and CAT). Similar to these data, exendin-4 attenuated oxidative stress and apoptosis in DC and I/R-injured hearts by increasing levels and expression of MnSOD and CAT [21, 38]. Also, GLP-1 and exendin-4 inhibited cell apoptosis in mice animal

◂**Fig. 3** Masson-trichrome staining of the left ventricles (LVs) of all groups of rats (**a**), mRNA (**b**), protein levels (**c**), collagen I and collagen III in LVs of all groups of rats. **a** Images I were II were taken from the sham-operated and sham + exendin-4-treated rats, respectively, and show normal myocardial tissue with normal striated heart muscle fibers (MF) and very few collagen fibers (CF) between the intercellular spaces. Images III and IV were taken from MI-induced rats and show apoptotic myocardial tissue (MF) with degenerated heart muscle fibers and increase amounts of collagen fibers (CF) between the intercellular spaces. Image V was taken from MI + exendin-4-treated rats and showsimprovement of architecture of myocardium (MF) and very few collagen fibers (CF) between the intercellular spaces. Image VI was taken from an MI + exendin-4 + EX527-treated rat and shows increased collagen fibers between the intercellular spaces of the muscle fibers (MF). Those seen in MI-induced rats. **b**, **c** Data are presented as mean ± SD of $n = 10$ rats/group. *, **, *****: vs. sham at $P < 0.05$, $P. < 0.01$ and $P < 0.001$, respectively. $^{\#, \#\#, \#\#\#}$: vs. sham + exendin-4-treated rats at $P < 0.05$, $P < 0.01$, and $P < 0.001$, respectively. ^{SSS}: vs. MI-induced rats at $P < 0.001$. $^{\&\&\&}$: vs. MI + exendin-4-treated rats at $P < 0.001$. EX527: a selective SIRT1 inhibitor

models of MI and HF. Interestingly, the increments in Bcl-2 and anti-oxidant enzymes and downregulation of Bax were also shown in the LVs of sham-operated rats co-treated with exendin-4 with no alteration of levels of ROS. Such data suggest a direct regulatory role of exendin-4 on these parameters rather than being secondary to its inhibitory effect on ROS generation.

However, the regulation of cellular anti-oxidants, apoptotic, and anti-apoptotic genes is very complicated and involves numerous pathways. Under stress and inflammatory conditions, NF-κB can directly induce apoptosis by upregulation of Bax [39, 40]. Also, TNF-α can induce cell apoptosis by inhibiting Bcl-2 levels through the ASK1/JNK pathway [41]. Furthermore, SIRT1 is a survival molecule that inhibits Bax upregulation and activation through the deacetylation of P53 [42]. Also, SIRT1 can upregulate anti-oxidant and anti-apoptotic genes through the deacetylation of Nrf-2 and FOXO transcription factors [28, 43]. In addition, SIRT1 can inhibit cell apoptosis and inflammation by direct nuclear deacetylation of NF-κB p65 [44].

Interestingly, and as discussed below, the significant reduction in the activity of NF-κB p65 and synthesis of TNF-α, as well as the upregulation and activation of SIRT1 in the heart MI + exendin-4-treated rats may explain such anti-oxidant and ant apoptotic potentials of exendin-4. Interestingly, the SIRT1 inhibitor, EX527 completely prevented these effects in the cardiomyocytes of these rats, an effect that was associated with reduced activity of NF-κB P65 and lower mRNA levels of TNF-α. Also, among all these parameters, only SIRT1 was upregulated in the hearts of the sham-operated rats. These data clearly show the anti-oxidant and anti-apoptotic effects of exendin-4 are mainly mediated by a SIRT-dependent mechanism. In addition, it was shown that SIRT1 improves mitochondria structure and biogenesis by activation of PGC-α1 [45]. Hence, the increment in SIRT1 levels in the hearts of MI rats after exendin-4 treatment may explain why these hearts have contact mitochondria and lower levels of ROS, which were completely reversed by EX527. However, if the protective effect of exendin-4 confers a direct effect on some ROS generating enzymes (e.g., NADPH oxidase, Myeloperoxidase) that are activated in the ischemic tissue [29] remains enigmatic and needs further investigation.

On the other hand, inflammation and subsequent fibrosis are the major pathophysiological mechanisms operating in the failing heart [1]. During the acute phase of MI, overproduction of ROS and the release of the Danger-Associated Molecular Pattern (DAMPs) and the pro-inflammatory cytokine (TNF-1α and IL-6) from ischemic myocardium initiates the inflammatory response (Suthahar et al. [1]). Subsequently, this induces fibroblast proliferation and turns them to an inflammatory phenotype which can secrete pro-inflammatory cytokines and chemoattractant molecules to recruit more circulatory leukocytes to the heart [1, 46, 47]. This crosstalk between fibroblast and macrophages perpetuate the pre-existing inflammation and increases the production of various pro-fibrotic molecules (e.g., TGFβ1) and metalloproteinase (MMPs), mainly from the neighboring macrophages [1]. TGFβ1 stimulates the myofibroblast to produce an excessive amount of collagen by acting through the Smad3 pathway [1, 48, 49]. On the other hand, the excessive production of MMPs and subsequent increase in the levels of tissue inhibitor of metalloproteinase (TIMP) from macrophages and other cardiac cells results in a long-term ongoing and sustained remodeling [50].

In the same line, the biochemical and microscopic evidence presented in this study showed active inflammation and fibrosis in the LVs of MI-induced rats that is characterized by excessive accumulation of collagen fibers between cardiomyocytes and increased mRNA and protein synthesis of collagen I/III and mRNA and levels of TNF-α and IL-6, as well as upregulation of TGFβ1 and Smad3. In addition, we also found increased protein levels of both MMP2 and MMP9. However, exendin-4 completely ameliorated all these events and significantly reduced collagen activation and deposition, suppressed the synthesis and release of TNF-α and IL-6, inhibited TGF-β1/Smad3 axis, and downregulated the levels of MMP2/9. Supporting our data, exendin-4 suppressed collagen I/III synthesis in female mice after 8 weeks post MI induction by reducing macrophage infiltration, inhibiting the release of inflammatory cytokines (IL-1β, IL-6), and suppressing TGF-β3/Smad3 signaling. Similar results were also shown in the DC hearts [27].

Nonetheless, NF-κB is upregulated in most of the cardiac cells during cardiac remodeling and has been identified as the master regulatory protein that stimulates the synthesis and the release of a wide range of inflammatory

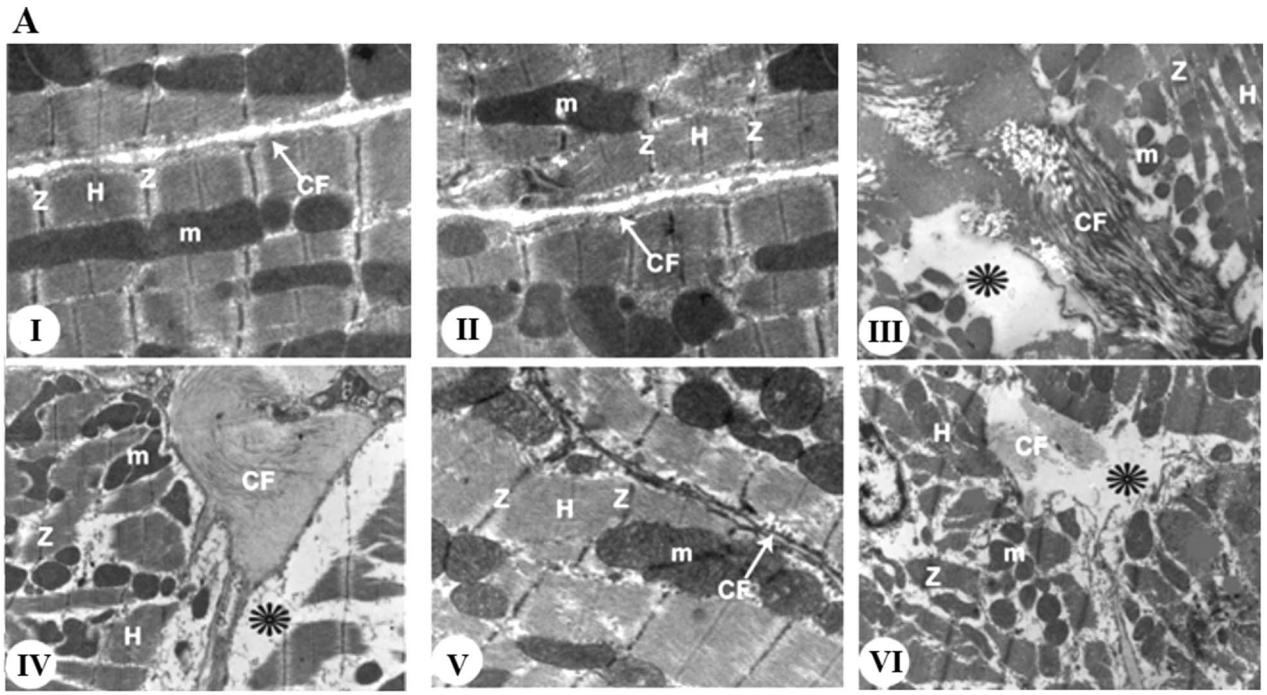
A
I
II
III
IV
V
VI
CF
m
Z
H

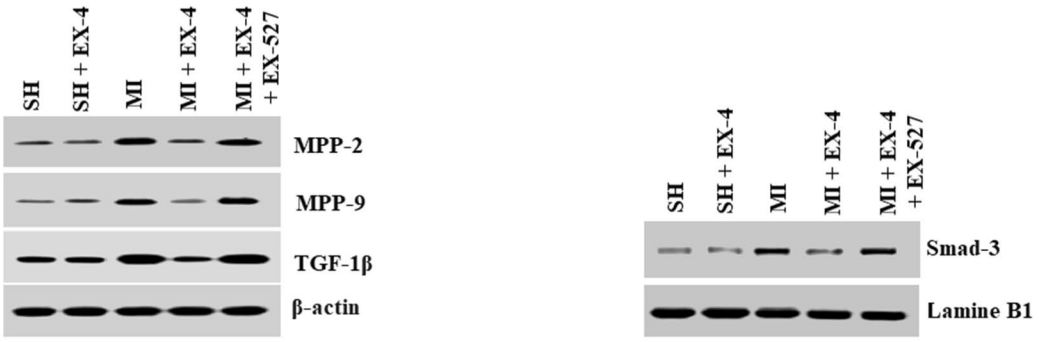
SH
SH + EX-4
MI
MI + EX-4
MI + EX-4 + EX-527
MPP-2
MPP-9
TGF-1β
β-actin
Smad-3
Lamine B1

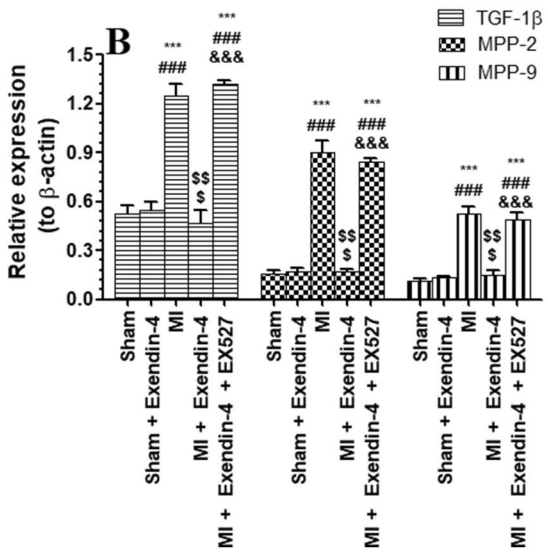
B
TGF-1β
MPP-2
MPP-9
Relative expression (to β-actin)
Sham
Sham + Exendin-4
MI
MI + Exendin-4
MI + Exendin-4 + EX527

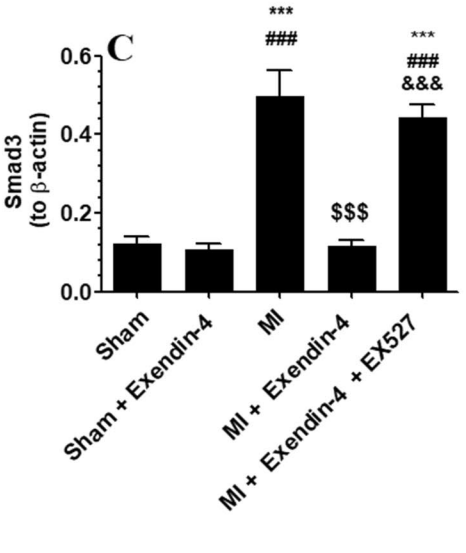
C
Smad3 (to β-actin)
Sham
Sham + Exendin-4
MI
MI + Exendin-4
MI + Exendin-4 + EX527

◂**Fig. 4** Transmission electron micrographs (TEM) of the left ventricles of all groups of rats (**a**) and protein levels of TGF-β1, MMP2, MMP9 (**b**), and Smad3 (**c**) in LVs of all groups of rats. **a** Images I and II were taken from the sham-operated and sham + exendin-4-treated rats, respectively, and normal myocyte structure with clear bands (Z and H) and mitochondria (m) and few collagen fibers (CF) between plasma membranes. Images III and IV were taken from MI-induced rats and shows fragmentation of myofibrils (asterisks) and muscle bands (Z and H), disintegrated mitochondria (m), and increasing amounts of collagen fibers (CF) in the very dilated intercellular between plasma membranes. Image V was taken from MI + exendin-4-treated rats and intact myocytes structure with clear bands (Z and H), mitochondria (m), and reduced collagen fibers (CF) between plasma membranes. **f** was taken from an MI + exendin-4 + EX527-treated rat and shows a similar picture to that seen in MI-induced rats. **b**, **c** Data are presented as mean ± SD of $n = 10$ rats/group. *****: vs. sham at $P < 0.001$. ###: vs. sham + exendin-4-treated rats at $P < 0.001$, respectively. ^{SSS}: vs. MI-induced rats at $P < 0.001$. &&&: vs. MI + exendin-4-treated rats at $P < 0.001$. EX527: a selective SIRT1 inhibitor

cytokines [51]. The activity of NF-κB depends on its nuclear translocation and nuclear post-translational modification including phosphorylation and acetylation [51]. As mentioned above, SIRT1 is one of the major deacetylases that controls the activity of NF-κB. Associated with the reduced levels of SIRT1 in the hearts of MI-induced rats, the nuclear levels, activation, and acetylation of NF-κB P65were significantly increased but were normalized in MI-induced rats treated with exendin-4, an effect that was completely prevented by co-treatment with EX527. Based on this we concluded that the Anti-inflammatory effect of SIRT1 is mediated by inhibition of NF-κB and is also SIRT1 dependent. Although it is a new observation in the hearts of MI-induced rats, these data are supported by other pieces of evidence of cancer cells and inflammatory macrophage-derived insulin resistance where exendin-4 showed protection mainly by inhibiting macrophage infiltration and the release of inflammatory cytokines mainly by inhibiting NF-kB [52, 53].

During the last decades, the emerging role of PARP1 in the pathogenesis of cardiac apoptosis, dysfunction, and remodeling post MI and in HF is receiving much attention [7–9, 16–18, 36]. During the DNA repair mechanism, activation of PARP1 was shown to deplete intracellular NAD^+ which leads to energy insufficiency and induction of apoptosis [54, 55]. As it utilizes NAD^+ as a substrate, it was shown that over-activation of PAPRP1 can induce cell death and activation of NF-κB by inhibiting SIRT1 synthesis and activity [12, 55]. Also and independent of its enzymatic activity, PARP1 is a potent coactivator of NF-κB that stimulates the inflammatory environment by interacting with p300 to provide additional interaction sites for p50 on p300 [14]. Indeed, PARP1 deficient mice have reduced expression of NF-κB-dependent inflammatory genes and are protected against serval inflammatory disorders including the adverse remodeling post MI. On the contrary, it was shown that SIRT1 not only suppresses the activity of PAPR-1 by deacylation but also inhibits its transcription [12]. This creates an opposite relationship between PARP1 and SIRT1.

PARP1 levels and activities were significantly increased, whereas SIRT1 levels were significantly depressed in animal models of MI animal model [3, 28]). These findings were also shown in this study where the activity, mRNA and protein levels and acetylation rate of PARP1 where significantly increases but the activity, mRNA, and protein levels of SIRT1 were significantly decreased in the LVs of MI-induced rats. Interestingly, there was a significant and strong interaction between PARP1 and p300 and weak interaction between PARP1 and SIRT1 in the LVs of these hearts. This could be due to reduced expression levels of SIRT1 and clearly explain why the hearts of these rats have sustained activation of NF-κB p65. However, the most novel finding in this study is that we found a completely opposite picture in the hearts of both control and MI-induced rats which showed increased activity and levels of SIRT1, reduced activity, levels and acylation of PARP1 and reduced PARP1 activation, which were prevented by EX527. Accordingly, and in addition to a direct inhibitory effect on p65, we concluded that the anti-inflammatory effect of exendin-4 is also triggered by SIRT1-induced deacetylation and reduced synthesis of PAPR-1 which subsequently reduced the interaction of PARP1 with p300 and so inhibiting the activity of NF-κB p65 p65 and reduced synthesis.

However, in spite of these findings, this study still has some limitations. Although we have shown that exendin-4 inhibits the activity of PARP1 through activation of SIRT, the opposite could be also correct and cannot be concluded

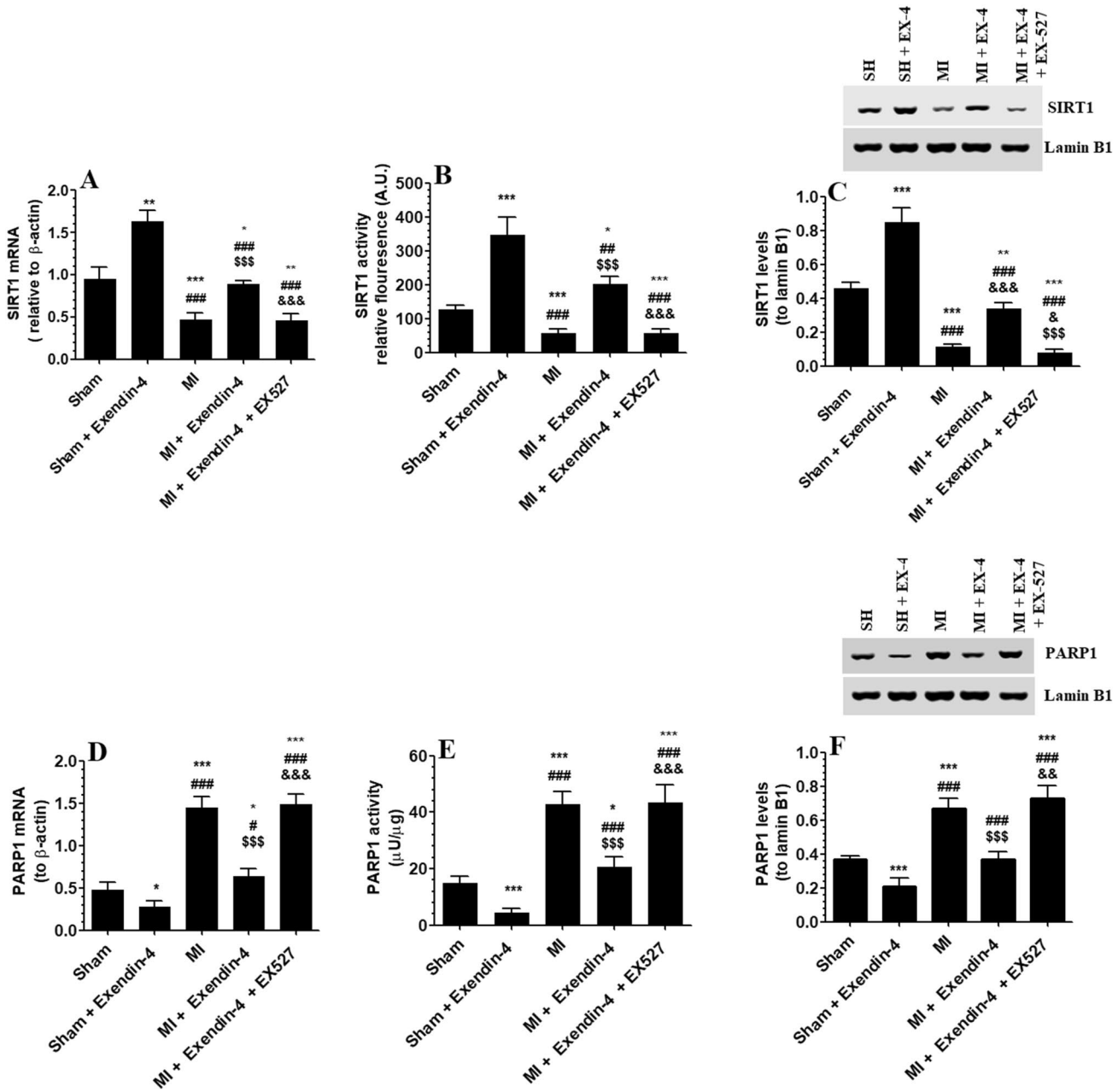

Fig. 5 mRNA, activity, and protein levels of SIRT1 (A-C, respectively) and PARP1 (D-F, respectively) in the left ventricles (LVs) of all groups of rats. Data are presented as mean ± SD of $n = 10$ rats/group. *, **, *****: vs. sham at $P < 0.05$, $P < 0.01$ and $P < 0.001$, respectively. $^{\#, \#\#, \#\#\#}$: vs. sham + exendin-4-treated rats at $P < 0.05$, $P < 0.01$, and 0.001, respectively. ^{SSS}: vs. MI-induced rats at $P < 0.001$. $^{\&\&\&}$: vs. MI + exendin-4-treated rats at $P < 0.001$. EX527: a selective SIRT1 inhibitor

in this study. Hence further experiments using PARR1 deficient animals may clearly answer this question. In addition, most of the cardiac cells including fibroblasts, macrophages, cardiomyocytes can synthesize PARP1 and NF-κB and secretes inflammatory cytokines and other pro-fibrotic factors. Another limitation in this study is that these effects are shown in total cell extracts so we were unable to identify which precise type of cardiac cells was affected by exendin-4. Such information requires more cell culture evidence.

In conclusion, the data in our hands are still very interesting and first in literature that showed a protective effect of exendin-4 against cardiac remodeling post MI by modulating the activity of SIRT1 and PARP1 and subsequent reduction in the inflammatory response.

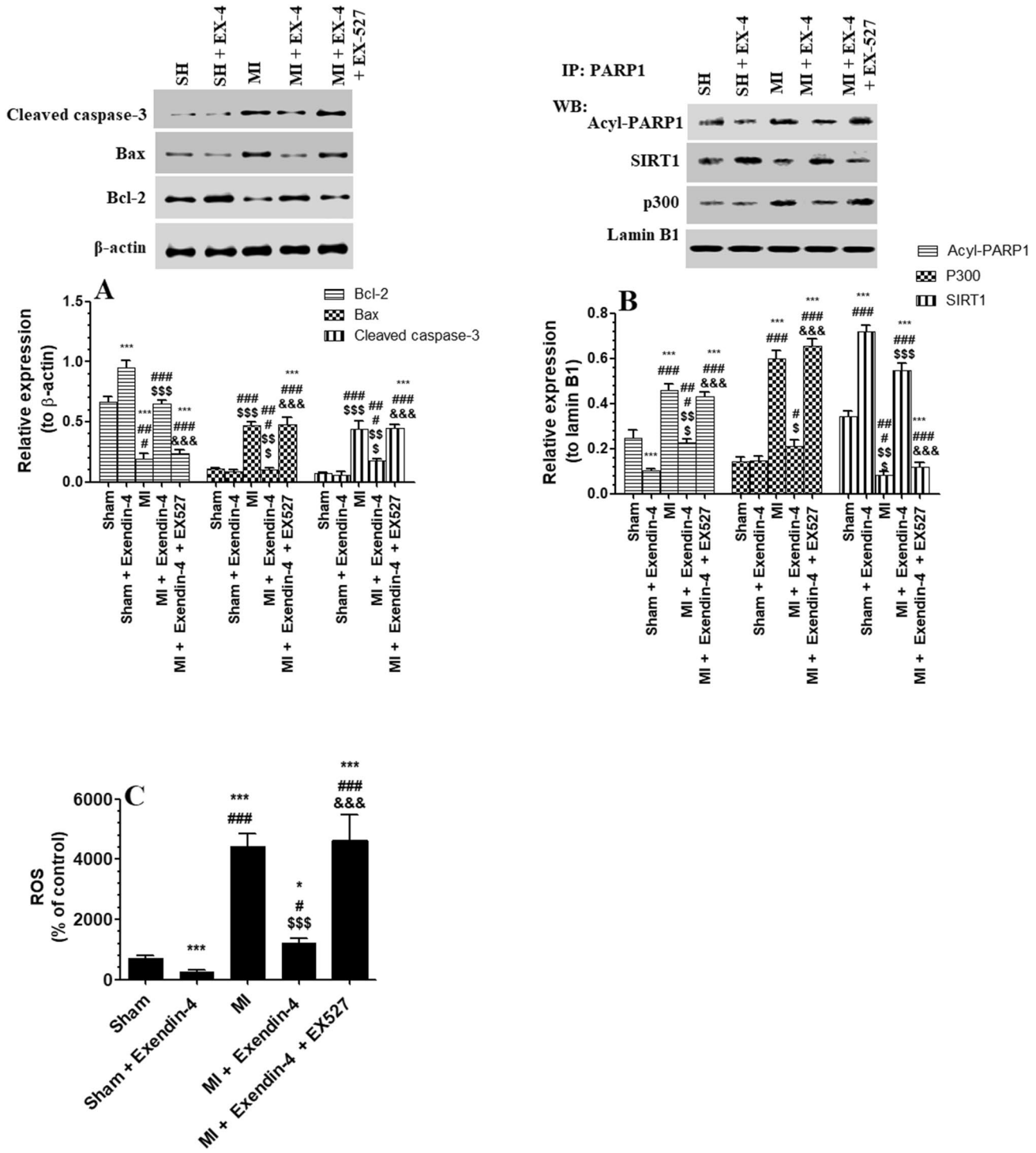

Fig. 6 Protein levels of Bax, Bcl-2, and cleaved-3 (**a**–**c**, respectively) and protein levels of acyl-PARP1, p300, and SIRT1 (**b**), as well as levels of reactive oxygen species (ROS) (**c**) in the left ventricles (LVs) of all groups of rats. **b** Proteins were first immunoprecipitated with PARP1 antibody and then blotted with antibodies against acyl-APRP1, SIRT1, and p300. Data are presented as mean ± SD of $n = 10$ rats/group. *, ***: vs. sham at $P < 0.05$ and $P < 0.001$, respectively. $^{\#,\#\#,\#\#\#}$: vs. sham + exendin-4-treated rats at $P < 0.05$ and 0.001, respectively. $^{\$,\$\$\$}$: vs. MI-induced rats at $P < 0.05$ and $P < 0.001$, respectively. $^{\&\&\&}$: vs. MI + exendin-4-treated rats at $P < 0.001$. EX527: a selective SIRT1 inhibitor

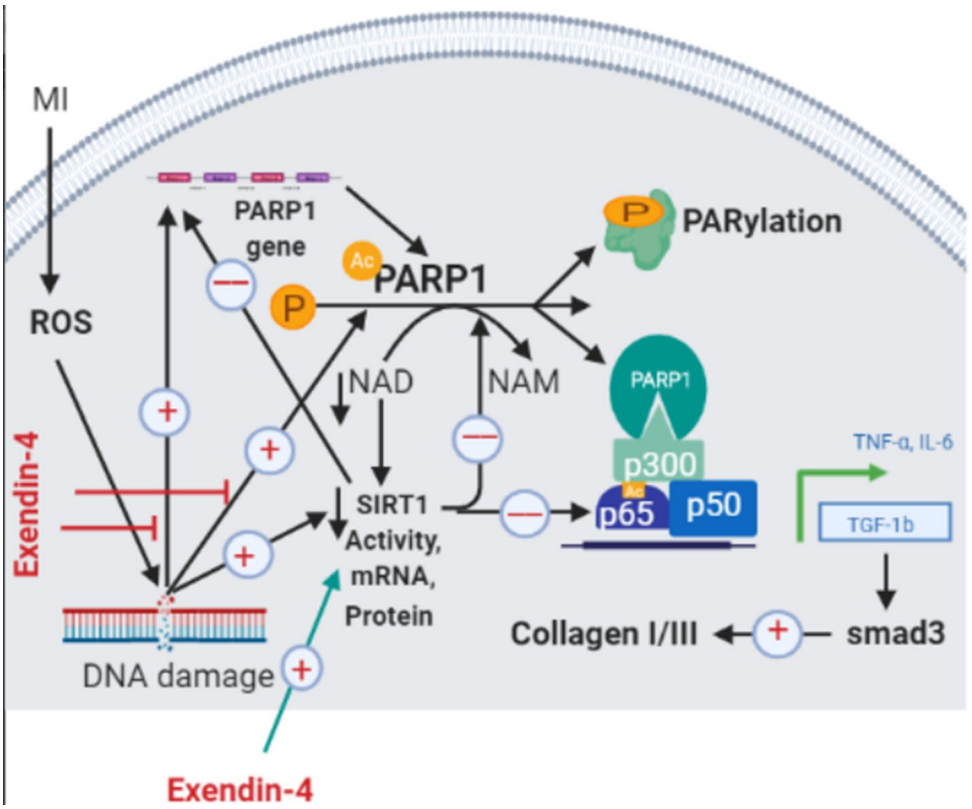

Fig. 7 Graphical presentation of the effect of exendin-4 against myocardial infarction (MI)-induced cardiac remodeling. Under ischemic conditions, ROS and other stress factors induce DNA damage that elaborates the mRNA and protein levels of PARP1 and increases PARP1 acetylation. In turn, over-activation of PARP1 depletes levels of NAD^+ which is a major substrate of SIRT1, thus promoting inhibition of SIRT1 and a further increase in PARP1 and NF-κB 65 acetylation. In addition, MI inhibits mRNA and protein synthesis of SIRT1. Acetylated PARP1 also interacts with p300 to facilitate the activity of p65 and hence increasing the expression of the inflammatory cytokines (e.g., TNF-α and IL-6). In addition, the sustained activity of NF-κ-B p65 and the other inflammatory cytokines promote the synthesis and release of TGFβ1 which acts through Smad3 in the myofibroblasts to increase collagen synthesis and deposition. In one way, it could be possible that exendin-4 can act by decreasing DNA damage, thus inhibiting PARP1 activation, transcription, and signaling which ultimately leads to activation of SIRT1. Also, and most likely, exendin-4 increases mRNA and protein levels and activity of SIRT1 which in turn inhibits PARP1 activity by deacetylation. Furthermore, exendin-4 is able to inhibit PARP1 transcription levels and activity by consuming most of NAD^+ in the cell leading to levels and the transcription and translation of PARP

Acknowledgements The authors extend their appreciation to the Deanship of Scientific Research at King Khalid University for funding this work through research groups program under Grant Number (R.G.P. 1/40/40).

Author contributions RE obtained the fund. RE, HAD, SA , AAA, and SME designed the experimental procedure and drafted the proposal. MAE, RE and FE established the animal model and collected samples and blood. RE, AFE, MSAZ, MAS, FE, MAE performed the biochemical analysis and histopathology and electron microscopy studies. RE, AAA, SME HAD, and SA drafted the final version of the manuscript.

Funding This work is fully funded by Deanship of Scientific Research at King Khalid University for funding this work through research groups program under Grant Number (R.G.P. 1/40/40).

Compliance with Ethical Standards

Conflict of interest Authors Refaat A Eid, Samah A Alharbi, Attalla Farag El-kott, Samy M Eleawa, Mohamed Samir Ahmed Zaki, Fahmy El-Sayed, Muhammad Alaa Eldin, Hussain Aldera, and Abd Al-Rahman Salem Alshudiefat declare that they havo no conflicts of interest.

Ethical Approval All applicable international, national, and/or institutional guidelines for the care and use of animals were followed.

References

1. Suthahar, N., Meijers, W. C., Silljé, H. H., & de Boer, R. A. (2017). From inflammation to fibrosis—Molecular and cellular mechanisms of myocardial tissue remodelling and perspectives on differential treatment opportunities. *Current Heart Failure Reports, 14*, 235–250.

2. Schirone, L., Forte, M., Palmerio, S., Yee, D., Nocella, C., Angelini, F., et al. (2017). A review of the molecular mechanisms underlying the development and progression of cardiac remodeling. *Oxidative Medicine and Cellular Longevity, 2017*, 3920195.
3. Hill, J. A., & Olson, E. N. (2008). Cardiac plasticity. *New England Journal of Medicine, 358*, 1370–1380.
4. Ohtani, T., Mohammed, S. F., Yamamoto, K., Dunlay, S. M., Weston, S. A., Sakata, Y., et al. (2012). Diastolic stiffness as assessed by diastolic wall strain is associated with adverse remodelling and poor outcomes in heart failure with preserved ejection fraction. *European Heart Journal, 33*, 1742–1749.
5. Burchfield, J. S., Xie, M., & Hill, J. A. (2013). Pathological ventricular remodeling: Mechanisms: Part 1 of 2. *Circulation, 128*, 388–400.
6. Pacher, P., Liaudet, L., Bai, P., Virag, L., Mabley, J., Hasko, G., et al. (2002). Activation of poly (ADP-ribose) polymerase contributes to development of doxorubicin-induced heart failure. *Journal of Pharmacology and Experimental Therapeutics, 300*, 862–867.
7. Szabo, C. (2005). Pharmacological inhibition of poly (ADP-ribose) polymerase in cardiovascular disorders: Future directions. *Current Vascular Pharmacology, 3*, 301–303.
8. Wang, J., Hao, L., Wang, Y., Qin, W., Wang, X., Zhao, T., et al. (2015). Inhibition of poly (ADP-ribose) polymerase and inducible nitric oxide synthase protects against ischemic myocardial damage by reduction of apoptosis. *Molecular Medicine Reports, 11*, 1768–1776.
9. Sun, S., Hu, Y., Zheng, Q., Guo, Z., Sun, D., Chen, S., et al. (2019). Poly (ADP-ribose) polymerase 1 induces cardiac fibrosis by mediating mammalian target of rapamycin activity. *Journal of Cellular Biochemistry, 120*, 4813–4826.
10. Ling, X. X., Liu, J. X., Lin, Y., Du, Y. J., Chen, S. Q., Chen, J. L., et al. (2016). Poly(ADP-ribosyl)ation of apoptosis antagonizing transcription factor involved in hydroquinone-induced DNA damage response. *Biomedical and Environmental Sciences, 29*, 80–84.
11. d'Amours, D., Desnoyers, S., d'Silva, I., & Poirier, G. G. (1999). Poly(ADP-ribosyl)ation reactions in the regulation of nuclear functions. *Biochemical Journal, 342*, 249.
12. Rajamohan, S. B., Pillai, V. B., Gupta, M., Sundaresan, N. R., Birukov, K. G., Samant, S., et al. (2009). SIRT1 promotes cell survival under stress by deacetylation-dependent deactivation of poly (ADP-ribose) polymerase 1. *Molecular and Cellular Biology, 29*, 4116–4129.
13. Szabo, C., Zingarelli, B., O'Connor, M., & Salzman, A. L. (1996). DNA strand breakage, activation of poly (ADP-ribose) synthetase, and cellular energy depletion are involved in the cytotoxicity of macrophages and smooth muscle cells exposed to peroxynitrite. *Proceedings of the National Academy of Sciences, 93*, 1753–1758.
14. Hassa, P., & Hottiger, M. (2002). The functional role of poly (ADP-ribose) polymerase 1 as novel coactivator of NF-κB in inflammatory disorders. *Cellular and Molecular Life Sciences, 59*, 1534–1553.
15. Yao, L., Huang, K., Huang, D., Wang, J., Guo, H., & Liao, Y. (2008). Acute myocardial infarction induced increases in plasma tumor necrosis factor-α and interleukin-10 are associated with the activation of poly (ADP-ribose) polymerase of circulating mononuclear cell. *International Journal of Cardiology, 123*, 366–368.
16. Halmosi, R., Deres, L., Gal, R., Eros, K., Sumegi, B., & Toth, K. (2016). PARP inhibition and postinfarction myocardial remodeling. *International Journal of Cardiology, 217*, S52–S59.
17. Jia, G., Zao, M., & Liu, X. (2017). Protective effect of diethylcarbamazine inhibits NF-κB activation in isoproterenol-induced acute myocardial infarction rat model through the PARP pathway. *Molecular Medicine Reports, 16*, 1596–1602.
18. Hans, C. P., Zerfaoui, M., Naura, A. S., Catling, A., & Boulares, A. H. (2008). Differential effects of PARP inhibition on vascular cell survival and ACAT-1 expression favouring atherosclerotic plaque stability. *Cardiovascular Research, 78*, 429–439.
19. Eid, R. A., Zaki, M. S. A., Al-Shraim, M., Eleawa, S. M., El-kott, A. F., Al-Hashem, F. H., et al. (2018). Subacute ghrelin administration inhibits apoptosis and improves ultrastructural abnormalities in remote myocardium post-myocardial infarction. *Biomedicine & Pharmacotherapy, 101*, 920–928.
20. Drucker, D. J. (2016). The cardiovascular biology of glucagon-like peptide-1. *Cell Metabolism, 24*, 15–30.
21. Timmers, L., Henriques, J. P., de Kleijn, D. P., DeVries, J. H., Kemperman, H., Steendijk, P., et al. (2009). Exenatide reduces infarct size and improves cardiac function in a porcine model of ischemia and reperfusion injury. *Journal of the American College of Cardiology, 53*, 501–510.
22. Woo, J. S., Kim, W., Ha, S. J., Kim, J. B., Kim, S.-J., Kim, W.-S., et al. (2013). Cardioprotective effects of exenatide in patients with ST-segment–elevation myocardial infarction undergoing primary percutaneous coronary intervention: Results of exenatide myocardial protection in revascularization study. *Arteriosclerosis, Thrombosis, and Vascular Biology, 33*, 2252–2260.
23. Noyan-Ashraf, M. H., Shikatani, E. A., Schuiki, I., Mukovozov, I., Wu, J., Li, R.-K., et al. (2013). A glucagon-like peptide-1 analog reverses the molecular pathology and cardiac dysfunction of a mouse model of obesity. *Circulation, 127*, 74–85.
24. Aravindhan, K., Bao, W., Harpel, M. R., Willette, R. N., Lepore, J. J., & Jucker, B. M. (2015). Cardioprotection resulting from glucagon-like peptide-1 administration involves shifting metabolic substrate utilization to increase energy efficiency in the rat heart. *PLoS ONE, 10*, e0130894.
25. Li, J., Zheng, J., Wang, S., Lau, H. K., Fathi, A., & Wang, Q. (2017). Cardiovascular benefits of native GLP-1 and its metabolites: An indicator for GLP-1-therapy strategies. *Frontiers in Physiology, 8*, 15.
26. Robinson, E., Cassidy, R. S., Tate, M., Zhao, Y., Lockhart, S., Calderwood, D., et al. (2015). Exendin-4 protects against post-myocardial infarction remodelling via specific actions on inflammation and the extracellular matrix. *Basic Research in Cardiology, 110*, 20.
27. Tate, M., Robinson, E., Green, B. D., McDermott, B. J., & Grieve, D. J. (2016). Exendin-4 attenuates adverse cardiac remodelling in streptozocin-induced diabetes via specific actions on infiltrating macrophages. *Basic Research in Cardiology, 111*, 1.
28. Hsu, C.-P., Zhai, P., Yamamoto, T., Maejima, Y., Matsushima, S., Hariharan, N., et al. (2010). Silent information regulator 1 protects the heart from ischemia/reperfusion. *Circulation, 122*, 2170–2182.
29. Mao, S., Chen, P., Li, T., Guo, L., & Zhang, M. (2018). Tongguan capsule mitigates post-myocardial infarction remodeling by promoting autophagy and inhibiting apoptosis: Role of Sirt1. *Frontiers in Physiology, 9*, 589.
30. Minematsu, T., Huang, L., Ibuki, A., Nakagami, G., Akase, T., Sugama, J., et al. (2012). Altered expression of matrix metalloproteinases and their tissue inhibitors in matured rat adipocytes in vitro. *Biological Research for Nursing, 14*, 242–249.
31. Bai, J., Zhang, N., Hua, Y., Wang, B., Ling, L., Ferro, A., et al. (2013). Metformin inhibits angiotensin II-induced differentiation of cardiac fibroblasts into myofibroblasts. *PLoS ONE, 8*, e72120.
32. Sun, L., Liu, C., Xu, X., Ying, Z., Maiseyeu, A., Wang, A., et al. (2013). Ambient fine particulate matter and ozone exposures induce inflammation in epicardial and perirenal adipose tissues in rats fed a high fructose diet. *Particle and Fibre Toxicology, 10*, 43.
33. Seo, S., Lee, M.-S., Chang, E., Shin, Y., Oh, S., Kim, I.-H., et al. (2015). Rutin increases muscle mitochondrial biogenesis with

AMPK activation in high-fat diet-induced obese rats. *Nutrients, 7*, 8152–8169.
34. Yan, N., Liu, Y., Liu, S., Cao, S., Wang, F., Wang, Z., et al. (2016). Fluoride-induced neuron apoptosis and expressions of inflammatory factors by activating microglia in rat brain. *Molecular Neurobiology, 53*, 4449–4460.
35. Fusegawa, Y., Hashizume, H., Okumura, T., Deguchi, Y., Shina, Y., Ikari, Y., et al. (2006). Hypertensive patients with carotid artery plaque exhibit increased platelet aggregability. *Thrombosis Research, 117*, 615–622.
36. Zhao, H., Zhang, J., & Hong, G. (2018). Minocycline improves cardiac function after myocardial infarction in rats by inhibiting activation of PARP-1. *Biomedicine & Pharmacotherapy, 97*, 1119–1124.
37. Harvey, A. P., & Grieve, D. J. (2014). Reactive oxygen species (ROS) signaling in cardiac remodeling and failure. In I. Laher (Ed.), *Systems biology of free radicals and antioxidants* (pp. 951–992). Berlin: Springer.
38. Bai, S., He, C., Zhang, K., Ding, X., Zeng, Q., Wang, J., et al. (2019). Effects of dietary inclusion of Radix Bupleuri and Radix Astragali extracts on the performance, intestinal inflammatory cytokines expression, and hepatic antioxidant capacity in broilers exposed to high temperature. *Animal Feed Science and Technology, 259*, 114288.
39. Shou, Y., Li, N., Li, L., Borowitz, J. L., & Isom, G. E. (2002). NF-κB-mediated up-regulation of Bcl-XS and Bax contributes to cytochrome c release in cyanide-induced apoptosis. *Journal of Neurochemistry, 81*, 842–852.
40. Gupta, S., Afaq, F., & Mukhtar, H. (2002). Involvement of nuclear factor-kappa B, Bax and Bcl-2 in induction of cell cycle arrest and apoptosis by apigenin in human prostate carcinoma cells. *Oncogene, 21*, 3727.
41. Matsuzawa, A., Nishitoh, H., Tobiume, K., Takeda, K., & Ichijo, H. (2002). Physiological roles of ASK1-mediated signal transduction in oxidative stress-and endoplasmic reticulum stress-induced apoptosis: Advanced findings from ASK1 knockout mice. *Antioxidants and Redox Signaling, 4*, 415–425.
42. Vaziri, H., Dessain, S. K., Eaton, E. N., Imai, S.-I., Frye, R. A., Pandita, T. K., et al. (2001). hSIR2SIRT1 functions as an NAD-dependent p53 deacetylase. *Cell, 107*, 149–159.
43. Chong, A.-Y., & Lip, G. Y. (2002). Hormone replacement therapy and cardiovascular risk. *Treatments in Endocrinology, 1*, 95–103.
44. Kim, H. J., Joe, Y., Yu, J. K., Chen, Y., Jeong, S. O., Mani, N., et al. (2015). Carbon monoxide protects against hepatic ischemia/reperfusion injury by modulating the miR-34a/SIRT1 pathway. *Biochimica et Biophysica Acta, 1852*, 1550–1559.
45. Di, W., Lv, J., Jiang, S., Lu, C., Yang, Z., Ma, Z., et al. (2018). PGC-1: The energetic regulator in cardiac metabolism. *Current Issues in Molecular Biology, 28*, 29–46.
46. Fredj, S., Bescond, J., Louault, C., Delwail, A., & LecronPotreau, J. C. D. (2005). Role of interleukin-6 in cardiomyocyte/cardiac fibroblast interactions during myocyte hypertrophy and fibroblast proliferation. *Journal of Cellular Physiology, 204*, 428–436.
47. Pellman, J., Zhang, J., & Sheikh, F. (2016). Myocyte-fibroblast communication in cardiac fibrosis and arrhythmias: Mechanisms and model systems. *Journal of Molecular and Cellular Cardiology, 94*, 22–31.
48. Bujak, M., & Frangogiannis, N. G. (2007). The role of TGF-β signaling in myocardial infarction and cardiac remodeling. *Cardiovascular Research, 74*, 184–195.
49. Gong, D., Shi, W., Yi, S.-J., Chen, H., Groffen, J., & Heisterkamp, N. (2012). TGFβ signaling plays a critical role in promoting alternative macrophage activation. *BMC Immunology, 13*, 31.
50. DeLeon-Pennell, K. Y., Meschiari, C. A., Jung, M., & Lindsey, M. L. (2017). Matrix metalloproteinases in myocardial infarction and heart failure. *Progress in Molecular Biology and Translational Science, 147*, 75–100.
51. Kawano, S., Kubota, T., Monden, Y., Tsutsumi, T., Inoue, T., Kawamura, N., et al. (2006). Blockade of NF-κB improves cardiac function and survival after myocardial infarction. *American Journal of Physiology-Heart and Circulatory Physiology, 291*, H1337–H1344.
52. Guo, C., Huang, T., Chen, A., Chen, X., Wang, L., Shen, F., et al. (2016). Glucagon-like peptide 1 improves insulin resistance in vitro through anti-inflammation of macrophages. *Brazilian Journal of Medical and Biological Research, 49*(12), e5826.
53. Iwaya, C., Nomiyama, T., Komatsu, S., Kawanami, T., Tsutsumi, Y., Hamaguchi, Y., et al. (2017). Exendin-4, a glucagonlike peptide-1 receptor agonist, attenuates breast cancer growth by inhibiting NF-κ B activation. *Endocrinology, 158*, 4218–4232.
54. De Flora, A., Zocchi, E., Guida, L., Franco, L., & Bruzzone, S. (2004). Autocrine and paracrine calcium signaling by the CD38/NAD+/cyclic ADP-ribose system. *Annals of the New York Academy of Sciences, 1028*, 176–191.
55. Kauppinen, T. M., Gan, L., & Swanson, R. A. (2013). Poly(ADP-ribose) polymerase-1-induced NAD+ depletion promotes nuclear factor-κB transcriptional activity by preventing p65 de-acetylation. *Biochimica et Biophysica Acta, 1833*, 1985–1991.